

From Three-Dimensional Flower-Like α -Ni(OH)₂ Nanostructures to Hierarchical Porous NiO Nanoflowers: Microwave-Assisted Fabrication and Supercapacitor Properties

Yang Ren and Lian Gao^{*†}

State Key Laboratory of High Performance Ceramics and Superfine Microstructure, Shanghai Institute of Ceramics, Chinese Academy of Sciences, Shanghai 200050, China

A facile method is presented to prepare flower-like α -Ni(OH)₂ involving only microwave heating of nickel nitrate hydrate in ethanol solvent without any hard/soft templates or precipitate-controlling agents. After calcination procedure, hierarchical and porous NiO nanoflowers with large BET-specific surface areas and controlled pore-size distributions are readily fabricated. A possible formation mechanism is proposed based on self-assembly under microwave heating. The structure, morphology, and crystalline phase of the products are characterized by transmission electron microscopy (TEM), X-ray diffraction, thermogravimetric analysis, Fourier transform infrared spectroscopy, and N₂ adsorption/desorption isotherm analysis. TEM reveals that the obtained NiO nanoflowers have uniform size and are composed of sheet-like petals that are built up from nanocrystals. The resultant NiO nanostructures present a specific capacitance as high as 277 F/g and good cycling stability.

I. Introduction

CONTROLLING the architecture of inorganic nanocrystals has been of great research interest due to their unique shape- and size-dependent properties.^{1,2} NiO material, as an important functional oxide, has great potential applications as energy storage device, catalysis, magnetic semiconductor, etc.^{3–5} Many strategies for fabricating NiO nanocrystals have been reported, including Ni-organic coordination complex intermediates,^{6,7} carbothermal reduction,⁸ Ni(OH)₂ precursor (hard templates or self-assembly approaches), etc.^{9–11} Among these strategies, the controlling Ni(OH)₂ architecture has attracted more attention not only because the flexibility in formation of complex 3D architecture as the precursor of NiO nanostructures,^{12–16} but also for their excellent electrochemical properties in rechargeable alkaline battery applications.¹⁷

Ni(OH)₂ has two polymorphs, α - and β -Ni(OH)₂. Both of them have a hexagonal-layered structure and tend to form thin flakes or platelets in shape. α -Ni(OH)₂ is a hydroxyl-deficient phase with interlayer anions and water molecules rather than stoichiometric composition in β -Ni(OH)₂.¹⁷ For the distinguishing structure feature, α -Ni(OH)₂ show superior electrochemical properties than β -Ni(OH)₂, but hard to be prepared due to its easy phase transformation to β -form.¹⁷ So far, there are several methods to obtain α -Ni(OH)₂, such as sonochemical precipita-

tion, hydrothermal reaction, and the “chimie douce” technique.^{18–22} However, there has been no report on the facile synthesis of controlled hierarchical α -Ni(OH)₂ nanostructures without any hard/soft templates or precipitate-controlling agents. Herein, we report a simple route to prepare flower-like α -Ni(OH)₂ involving only one chemical in one solvent. By microwave heating of nickel nitrate hydrate in ethanol solvent at 150°C for 15 min, high-quality flower-like α -Ni(OH)₂ can be obtained via a self-assembly process. Then, followed with a tunable calcination of α -Ni(OH)₂, hierarchical and porous NiO nanostructures with large BET-specific surface areas and controlled pore-size distributions are readily fabricated. Furthermore, electrochemical properties of obtained NiO nanostructures are tested using cyclic voltammetry (CV) measurements. A high specific capacitance of 277 F/g and good cycling stability can be achieved due to the unique architecture. The present simple way for α -Ni(OH)₂ and NiO nanocrystals with controlled architectures will promote their multifunctional applications and could be versatile for the preparation of other metal hydroxides/oxides.

II. Experimental Procedures

All chemicals were purchased from Shanghai Chemical Regent Co. (Shanghai, China) with analytical grade and used without further purification. Typically, 20 mmol Ni(NO₃)₂·6H₂O was dissolved in 30 mL anhydrous ethanol under magnetic stirring to get a 0.67 mol/L green transparent solution. The as-formed green transparent solution was then transferred into a 50 mL Teflon container. The vessel containing precursor solution was subjected to microwave heating maintained at 150°C for 15 min (heating rate: 25°C/min) and then cooled down naturally. Green precipitates were generated and separated by centrifugation and washed by ethanol several times, and then dried under vacuum at 60°C overnight. The as-prepared green precursors were calcinated at 300°, 350°, and 400°C for 1 h (heating rate: 1°C/min) in air, respectively. The obtained gray black powders were correspondingly noted as C3001, C3501, and C4001.

The microwave oven (2.45 GHz, maximum power 300 W) used was a focused single-mode microwave synthesis system (Discover, CEM, Matthews, NC). The phase composition of the samples was characterized by X-ray powder diffraction (XRD) (Rigaku D/max 2550 V, Tokyo, Japan, CuK α , λ = 1.54178 Å). The morphologies of the products were observed using a transmission electron microscope (TEM) (JEM200CX, JEOL, Tokyo, Japan) and scanning electron microscopy (SEM) (JSM 6700F, Tokyo, Japan). A Fourier transform infrared (FT-IR) (Nexus, Nicolet, Madison, WI) spectrometer was used to examine the chemical composition of the samples. TG analysis was conducted using a NETZSCH STA 449C apparatus with an air flow of 20 mL/min and a heating rate of 10 K/min. Nitrogen adsorption/desorption isotherms were obtained at 77 K with a Micromeritics ASAP 2010 micropore analysis system

S. Suib—contributing editor

Manuscript No. 28215. Received June 21, 2010; approved July 20, 2010.

This work was financially supported by the National Key Basic Research Development Program of China (973 Program, 2005CB623605), the Shanghai Nanotechnology Promotion Center (No. 0852nm01900), and National Natural Science Foundation of China (Grant No. 50972157, 50672112).

^{*}Member, The American Ceramic Society.

[†]Author to whom correspondence should be addressed. e-mail: liangao@mail.sic.ac.cn

(Micrometitics, Norcross, GA). Specific surface areas were obtained by the BET method, and average pore diameters were determined using the Barrett–Joyner–Halenda method.

The electrochemical measurements were carried out using three-electrode cell system with Pt wire as counter electrode and saturated calomel electrode as reference electrode. The working electrode consisted of NiO products, acetylene black conductors, and polyvinylidene fluoride in an 80:10:10 weight ratio. The electrolyte used was 2M KOH aqueous solution. CV measurements were carried out using electrochemical workstation (Parstat 2273, Princeton Applied Research Co. Ltd., Oak Ridge, TN) in the scan range of -0.2 to 0.5 V.

III. Results and Discussion

The morphologies of as-prepared green powder are exhibited in Figs. 1(a)–(b). SEM image (Fig. 1(a)) clearly shows that the as-prepared precursor is composed of well-defined particles with flower-like shape. The particles are uniform in size of ca. $1\ \mu\text{m}$. The inset of Fig. 1(a) exhibits that the flower-like architectures are assembled by several interconnected sheet-like petals with smooth surface and the thickness ca. $20\ \text{nm}$. The XRD pattern of the precursor (Fig. 1(c)) exhibits typical features of $\alpha\text{-Ni(OH)}_2$ evidenced by the strongest reflection at the low 2θ of 12.7° . All of the reflections are matched well with the standard pattern for nickel nitrate hydroxide (JCPDS 22-0752), indicating the obtained sample can be defined as nitrated $\alpha\text{-Ni(OH)}_2$. The lattice parameters, refined with the MDI Jade 5.0 program (reliability factors: $R = 6.59\%$), are $a = 0.312\ \text{nm}$ and $c = 0.692\ \text{nm}$. The FT-IR spectrum (Fig. 1(d)) further verifies the chemical species of $\alpha\text{-Ni(OH)}_2$ precursor. The broad bands at $(3580\text{--}3400\ \text{cm}^{-1})$ indicate the presence of hydroxyl groups and water molecules.²⁰ The peak around $1600\text{--}1640\ \text{cm}^{-1}$ is due to $\delta\text{-H}_2\text{O}$ vibration of the water molecule.²⁰ The interlayer nitrate anion

reveals its presence by a set of strong peaks in the range of $1503\text{--}980\ \text{cm}^{-1}$.¹⁹ Two peaks, which appear between $630\text{--}650$ and $460\text{--}490\ \text{cm}^{-1}$, correspond to $\delta\text{-OH}$ and $\nu\text{-NiO}$ vibrations, respectively.²⁰ From the TG analysis (the inset of Fig. 1(c)), the thermal decomposition behavior is generally in good agreement with previous reports of $\alpha\text{-Ni(OH)}_2$.²⁰ The onset of phase transformation from obtained flower-like $\alpha\text{-Ni(OH)}_2$ to NiO is indicated with the abrupt weight loss at around 270°C .

The XRD patterns of calcination samples, namely C3001, C3501, and C4001, are shown in Fig. 2(a). After calcination at 300°C for 1 h, cubic phase NiO can be well indexed (JCPDS 47-1049). Nevertheless, the appearance of an unknown amorphous peak, located at $10\text{--}20^\circ$, indicates that a trace amount of impurity still exists after calcination at 300°C for 1 h. While the calcination temperature is higher than 300°C (C3501 and C4001 in our case), the impurity disappears and pure cubic phase NiO samples can be obtained. The average crystalline sizes of samples C3001, C3501, and C4001 calculated from (200) diffraction peak by Scherrer's formula are 9.2, 10.5, and 18.4 nm, respectively. The above results suggest that the phase purity and particle size of NiO nanostructures can be readily controlled by calcination procedures. The morphology of calcination sample C3501 is showed in Fig. 2(b). The shape of calcination particles well inherits the flower-like architecture of the $\alpha\text{-Ni(OH)}_2$ precursor. However, the surface texture of NiO nanoflowers, as exhibited in Fig. 2(c), seems to be rough and grainy, which is quite different from that of $\alpha\text{-Ni(OH)}_2$ precursor. SAED pattern (inset in Fig. 2(c)) in the circle region of a petal manifests the polycrystalline nature of NiO nanoflowers. The high-magnification TEM image (Fig. 2(d)) reveals that the petals are made of well-defined nanoparticles of ca. $10\ \text{nm}$ in size (agree with the calculated results from Scherrer's formula), and pores nearly homogeneously distributed among these nanoparticles. A representative high-resolution TEM image is given to examine the

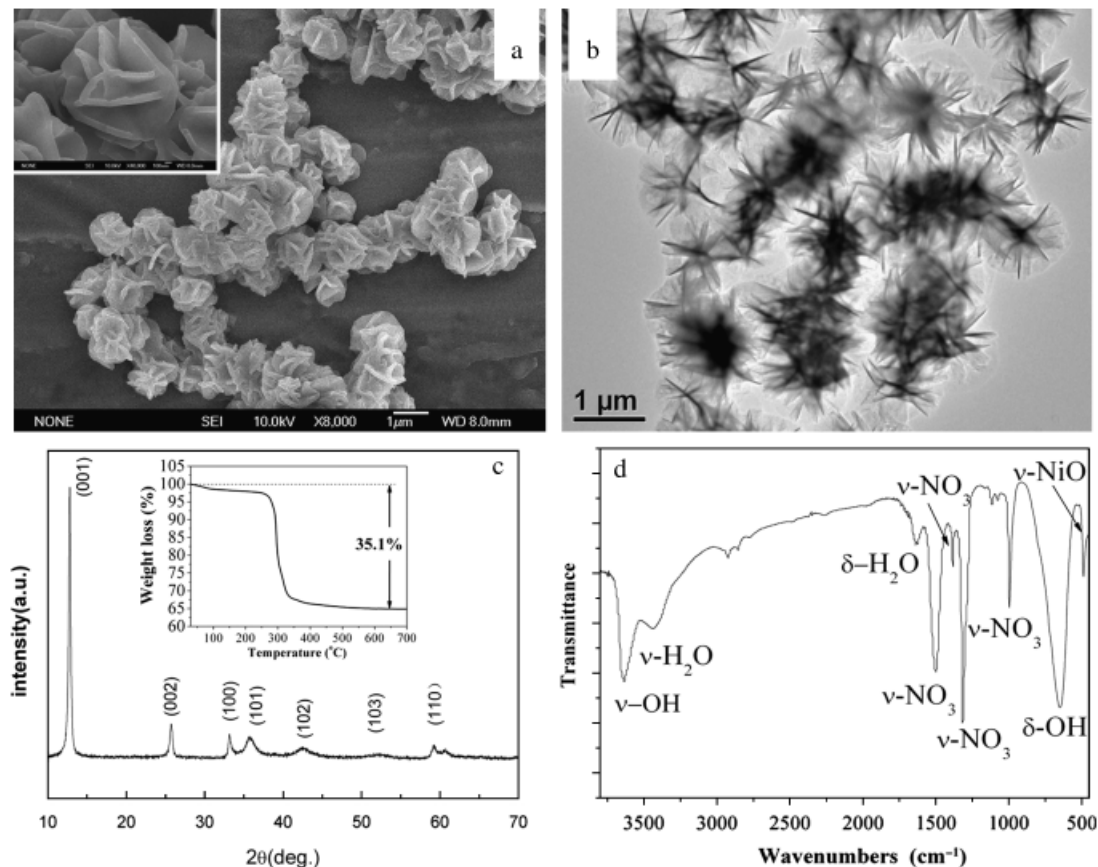


Fig. 1. (a) Scanning electron microscopic (SEM) image (the inset shows the close-up SEM image of an individual particle), (b) transmission electron microscopic image, (c) X-ray diffraction pattern (the inset shows the thermogravimetric curve of $\alpha\text{-Ni(OH)}_2$ precursor), and (d) Fourier transform infrared spectrum of the obtained flower-like $\alpha\text{-Ni(OH)}_2$ precursor.

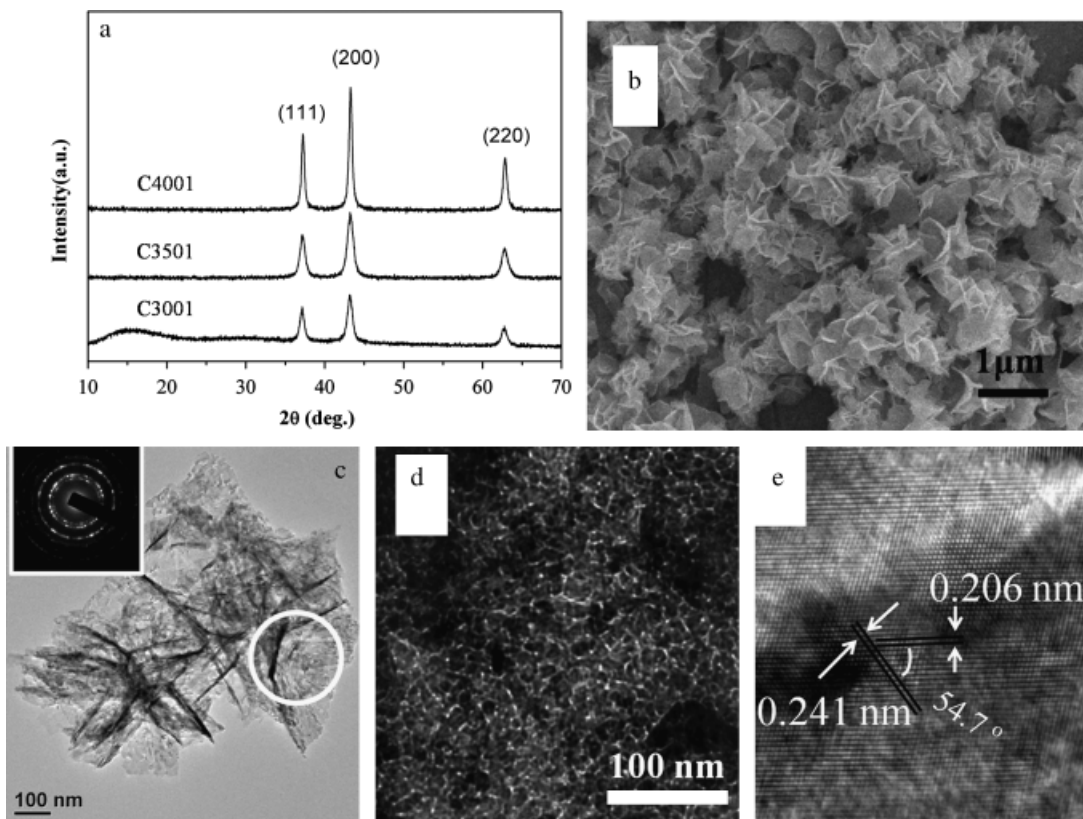
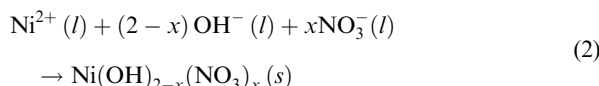
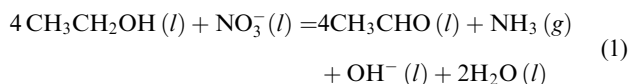


Fig. 2. (a) X-ray diffraction patterns of NiO products of C3001, C3501, and C4001, respectively, (b) scanning electron microscopic image, (c) low-magnification transmission electron microscopic (TEM) image (the inset shows the SAED pattern of circle region), (d) high-magnification TEM image, and (e) high-resolution TEM image of C3501 product.

interplanar distance of such nanoparticles. The lattice fringes with a spacing of 0.206 and 0.241 nm are well accord with the d -spacing of (111) and (200) plane of cubic phase NiO, and the dihedral angle of 54.7° further confirms that the resultant architectures are composed of NiO nanocrystals.

Figure 3(a) shows the nitrogen adsorption/desorption isotherms of pure-phase NiO samples C3501 and C4001. The hysteresis loop, appearing in the relative pressure (p/p_0) range of 0.45–1, indicates that the pore sizes in both NiO products are of mesoscale.²³ The specific surface area of the sample C3501 is $197 \text{ m}^2/\text{g}$ and a narrow pore-size distribution can be clearly observed with peak size at ca. 3.6 nm (Fig. 3(b)). On the other hand, as the annealing temperature increases to 400°C , the specific surface area of sample C4001 decreases to $97.2 \text{ m}^2/\text{g}$ and the peak size of pore distribution shifts to ca. 7.2 nm. This phenomenon should be attributed that the primary nanoparticles grow larger via thermal recrystallination of Ostwald-ripening mechanism. During this process, intercrystallited mesopores evolve into larger sized pores as the primary nanoparticles grow.^{24,25}

To explain the formation of hierarchical and porous NiO nanostructures, a possible formation mechanism based on experimental results is proposed. The thermodynamic process could be formulated as follows²⁶:



With microwave heating, the precursor solution goes through nucleation, aggregation, and ripening process. Namely, at the beginning, NO_3^- is quickly reduced by ethanol under microwave

heating and generates OH^- . Then, the released OH^- further reacts with Ni^{2+} and NO_3^- to create $\alpha\text{-Ni}(\text{OH})_2$ nuclei.²⁶ A large amount of nuclei burst and further grow into particles in larger sizes. At this stage, 2D nanosheets are readily to be formed as dominant morphology because of the layered structure feature of $\alpha\text{-Ni}(\text{OH})_2$ and proper monomer concentration. Subsequently, the produced primary nanosheets could assemble into 3D flower-like architecture due to crystal-face attraction, van der Waals forces and hydrogen bonds.^{27,28} Simultaneously, the particles could also heterogeneously nucleate and grow onto the petals of flower-like structure because of the continuous mass supply. Significantly, microwave heating helps to more quickly chemical reactions and facilitates the diffusion of the mass, which favors the stable growth of a flower-like $\alpha\text{-Ni}(\text{OH})_2$ with nanosheets as building blocks.²² Finally, after calcination, the flower-like $\alpha\text{-Ni}(\text{OH})_2$ transfer into highly porous NiO nanostructures with maintained morphology by the removal of interlayer anions.

Figure 4 shows the CV curves of pure NiO samples of C3501 and C4001. A couple of redox peaks in each curve clearly testifies the faradaic pseudocapacitive behavior of both NiO electrodes.²⁹ The specific capacitances (C_s) of C3501 and C4001 calculated from the CV curves according to the reported equation³⁰ are 277 and 182 F/g, respectively. Compared with the reported C_s value of NiO nanostructures prepared by molten salt, chemical precipitation, organic complex templates, oxalates precursor approaches, etc.,^{7,29,31–34} the obtained sample C3501 exhibits improved capacitance property. This notable improvement should be associated with the obtained hierarchical and porous nanostructures. The high BET surface area and appropriate pore channel are beneficial for the accessibility of electrolyte OH^- to the electrode active surface and a fast diffusion rate within the redox phase, which results in high specific capacitances.⁷ Besides, sample C3501 with large BET area and pore size at 3.6 nm obtained under lower calcination

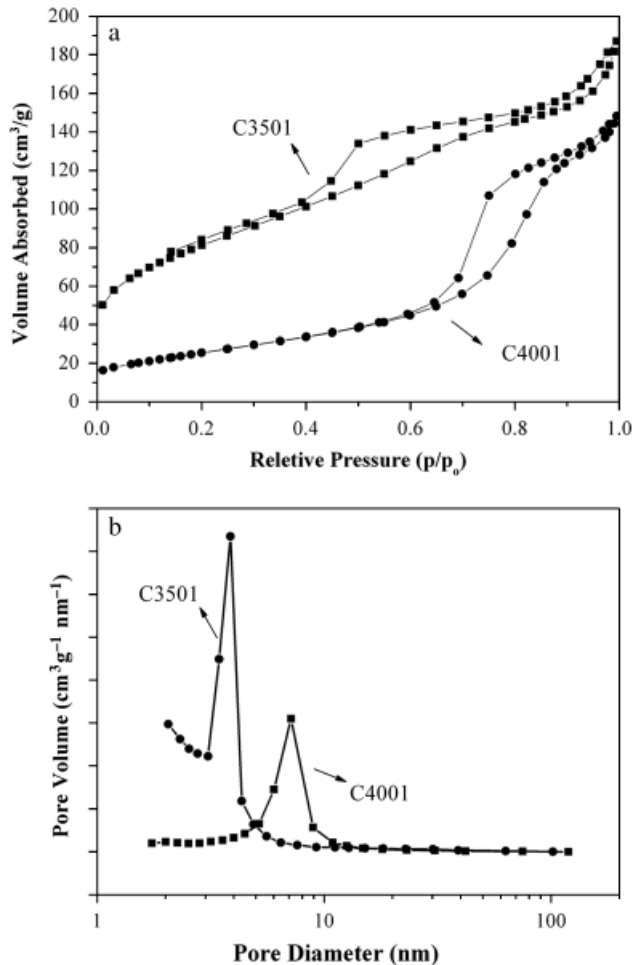


Fig. 3. (a) N₂ adsorption-desorption isotherms, and (b) Barrett-Joyner-Halenda desorption size-distribution plots of C3501 and C4001.

temperature possesses higher specific capacitance than that of C4001. This phenomenon indicates the increased crystal size, caused by calcination at higher temperature, leads to the decrease of specific surface area, accordingly reducing the capacitance properties.³⁰ Figure 5 gives the CV curves of sample C3501 working at different scanning rates. The shape of the CV curves well maintains the characteristic of pseudocapacitance redox course, indicating the prepared NiO electrode can work well at increased scanning rate. The corresponding specific capaci-

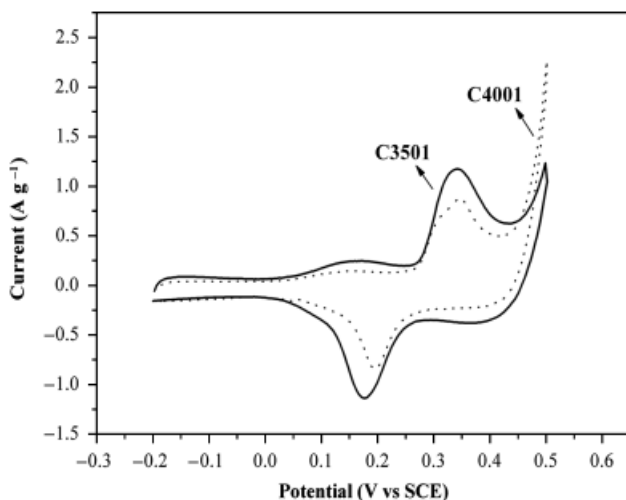


Fig. 4. Cyclic voltammetry curves of C3501 and C4001 products.

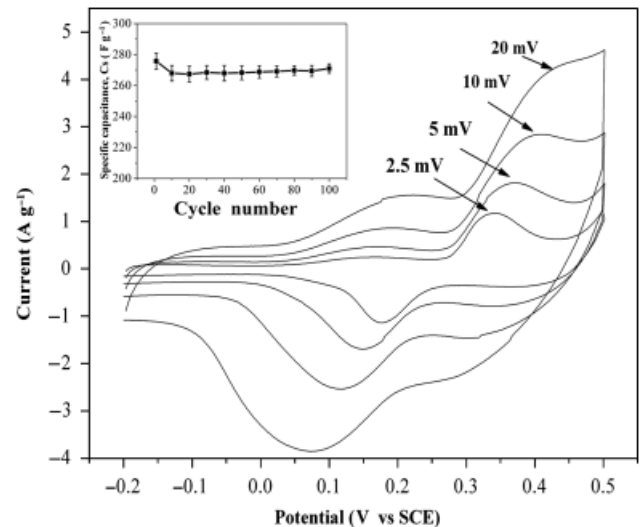


Fig. 5. Cyclic voltammetry curves of the C3501 obtained at different scan rates (the inset shows the variation of the specific capacitance with cycle number of C3501 at scan rate of 2.5 mV/s).

ties are as high as 265, 220, and 188 F/g with scan rate at 5, 10, and 20 mV/s, respectively. The inset of Fig. 5 shows the variation of the specific capacitance with cycle number at scan rate of 2.5 mV/s. After 100 cycles, a high specific capacitance of 271 F/g can be stabilized. This good cycling quality suggests that the as-obtained porous NiO nanoflowers have potential application in electrochemical supercapacitors.

IV. Conclusions

In summary, we report a facile method to prepare high-quality flower-like α -Ni(OH)₂ via self-assembly achieved by microwave heating of nickel nitrate hydrate in ethanol solvent at 150°C for 15 min. After calcination procedure, hierarchical and porous NiO nanocrystals with large specific surface areas of 197 m²/g and narrow pore distributions of 3.6 nm are readily fabricated. Electrochemical tests show that a high specific capacitance of 277 F/g and good cycling stability can be achieved due to the resultant NiO nanostructures. The present simple route for novel α -Ni(OH)₂ and NiO nanostructures should be extendable for the preparation of other metal hydroxide/oxide.

References

- Y. Cui and C. M. Lieber, "Functional Nanoscale Electronic Devices Assembled Using Silicon Nanowire Building Blocks," *Science*, **291**, 851-3 (2001).
- A. H. Lu and F. Schuth, "Nanocasting: A Versatile Strategy for Creating Nanostructured Porous Materials," *Adv. Mater.*, **18**, 1793-805 (2006).
- M. Yoshio, Y. Todorov, K. Yamato, H. Noguchi, J. Itoh, O. Masaki, and T. Mouri, "Preparation of Li_{1-x}Mn_xNi_{1-x-y}O₂ as a Cathode for Lithium-Ion Batteries," *J. Power Sources*, **74**, 46-53 (1998).
- R. Alcantara, P. Lavela, J. I. Tirado, R. Stoyanova, and E. Zhecheva, "Changes in Structure and Cathode Performance with Composition and Preparation Temperature of Lithium Cobalt Nickel Oxide," *J. Electrochem. Soc.*, **145**, 730-6 (1998).
- E. L. Miller and R. E. Rocheleau, "Electrochemical Behavior of Reactively Sputtered Iron-Doped Nickel Oxide," *J. Electrochem. Soc.*, **144**, 3072-7 (1997).
- X. F. Song and L. Gao, "Facile Synthesis of Polycrystalline NiO Nanorods Assisted by Microwave Heating," *J. Am. Ceram. Soc.*, **91**, 3465-8 (2008).
- C. C. Yu, L. X. Zhang, J. L. Shi, J. J. Zhao, J. H. Gao, and D. S. Yan, "A Simple Template-Free Strategy to Synthesize Nanoporous Manganese and Nickel Oxides with Narrow Pore Size Distribution, and their Electrochemical Properties," *Adv. Funct. Mater.*, **18**, 1544-54 (2008).
- X. Wang, L. Yu, P. Hu, and F. Yuan, "Synthesis of Single-Crystalline Hollow Octahedral NiO," *Cryst. Growth Des.*, **7**, 2415-8 (2007).
- S. A. Needham, G. X. Wang, and H. K. Liu, "Synthesis of NiO Nanotubes for Use as Negative Electrodes in Lithium ion Batteries," *J. Power Sources*, **159**, 254-7 (2006).
- D. B. Wang, C. X. Song, Z. S. Hu, and X. Fu, "Fabrication of Hollow Spheres and Thin Films of Nickel Hydroxide and Nickel Oxide with Hierarchical Structures," *J. Phys. Chem. B*, **109**, 1125-9 (2005).

- ¹¹X. F. Song and L. Gao, "Facile Synthesis and Hierarchical Assembly of Hollow Nickel Oxide Architectures Bearing Enhanced Photocatalytic Properties," *J. Phys. Chem. C*, **112**, 15299–305 (2008).
- ¹²W. Zhou, M. Yao, L. Guo, Y. M. Li, J. H. Li, and S. H. Yang, "Hydrazine-Linked Convergent Self-Assembly of Sophisticated Concave Polyhedrons of beta-Ni(OH)₂ and NiO from Nanoplate Building Blocks," *J. Am. Chem. Soc.*, **131**, 2959–64 (2009).
- ¹³J. Wang, H. Pang, J. Z. Yin, L. N. Guan, Q. Y. Lu, and F. Gao, "Controlled Fabrication and Property Studies of Nickel Hydroxide and Nickel Oxide Nanostructures," *Crystengcomm*, **12**, 1404–9 (2010).
- ¹⁴L. Liu, Y. Li, S. M. Yuan, M. Ge, M. M. Ren, C. S. Sun, and Z. Zhou, "Nanosheet-Based NiO Microspheres: Controlled Solvothermal Synthesis and Lithium Storage Performances," *J. Phys. Chem. C*, **114**, 251–5 (2010).
- ¹⁵X. Zhu, Z. Gui, Y. Y. Ding, Z. Z. Wang, Y. Hu, and M. Q. Zou, "A Facile Route to Oriented Nickel Hydroxide Nanocolumns and Porous Nickel Oxide," *J. Phys. Chem. C*, **111**, 5622–7 (2007).
- ¹⁶Y. Wang, Q. S. Zhu, and H. G. Zhang, "Fabrication of Beta-Ni(OH)₂ and NiO Hollow Spheres by a Facile Template-Free Process," *Chem. Commun.*, **41**, 5231–3 (2005).
- ¹⁷B. Mavis and M. Akinc, "Three-Component Layer Double Hydroxides by Urea Precipitation: Structural Stability and Electrochemistry," *J. Power Sources*, **134**, 308–17 (2004).
- ¹⁸H. J. Liu, T. Y. Peng, D. E. Zhao, K. Dai, and Z. H. Peng, "Fabrication of Nickel Oxide Nanotubes by Anionic Surfactant-Mediated Templating Method," *Mater. Chem. Phys.*, **87**, 81–6 (2004).
- ¹⁹B. H. Liu, S. H. Yu, S. F. Chen, and C. Y. Wu, "Hexamethylenetetramine Directed Synthesis and Properties of a New Family of Alpha-Nickel Hydroxide Organic-Inorganic Hybrid Materials with High Chemical Stability," *J. Phys. Chem. B*, **110**, 4039–46 (2006).
- ²⁰M. Taibi, S. Ammar, N. Jouini, F. Fievet, P. Molinie, and M. Drillon, "Layered Nickel Hydroxide Salts: Synthesis, Characterization and Magnetic Behaviour in Relation to the Basal Spacing," *J. Mater. Chem.*, **12**, 3238–44 (2002).
- ²¹P. Jeevanandam, Y. Kolytynin, and A. Gedanken, "Synthesis of Nanosized α -Nickel Hydroxide by a Sonochemical Method," *Nano Lett.*, **1**, 263–6 (2001).
- ²²L. P. Xu, Y. S. Ding, C. H. Chen, L. L. Zhao, C. Rimkus, R. Joesten, and S. L. Suib, "3D Flowerlike Alpha-Nickel Hydroxide with Enhanced Electrochemical Activity Synthesized by Microwave-Assisted Hydrothermal Method," *Chem. Mater.*, **20**, 308–16 (2008).
- ²³J. H. Huang and L. Gao, "Synthesis and Characterization of Porous Single-Crystal-Like In₂O₃ Nanostructures via a Solvothermal-Annealing Route," *J. Am. Ceram. Soc.*, **89**, 724–7 (2006).
- ²⁴H. C. Zeng, "Synthetic Architecture of Interior Space for Inorganic Nanostructures," *J. Mater. Chem.*, **16**, 649–62 (2006).
- ²⁵X. W. Lou, D. Deng, J. Y. Lee, and L. A. Archer, "Thermal Formation of Mesoporous Single-Crystal Co₃O₄ Nano-Needles and their Lithium Storage Properties," *J. Mater. Chem.*, **18**, 4397–401 (2008).
- ²⁶C. L. Tang, G. S. Li, and L. P. Li, "Fabrication of Nickel Nitrate Hydroxide Microsphere with Inheriting Morphology to beta-Ni(OH)₂ and NiO," *Chem. Lett.*, **37**, 1138–9 (2008).
- ²⁷L. S. Zhong, J. S. Hu, H. P. Liang, A. M. Cao, W. G. Song, and L. J. Wan, "Self-Assembled 3D Flowerlike Iron Oxide Nanostructures and their Application in Water Treatment," *Adv. Mater.*, **18**, 2426–31 (2006).
- ²⁸S. Y. Zeng, K. B. Tang, T. W. Li, Z. H. Liang, D. Wang, Y. K. Wang, Y. X. Qi, and W. W. Zhou, "Facile Route for the Fabrication of Porous Hematite Nanoflowers: Its Synthesis, Growth Mechanism, Application in the Lithium ion Battery, and Magnetic and Photocatalytic Properties," *J. Phys. Chem. C*, **112**, 4836–43 (2008).
- ²⁹Y. G. Wang and Y. Y. Xia, "Electrochemical Capacitance Characterization of NiO with Ordered Mesoporous Structure Synthesized by Template SBA-15," *Electrochim. Acta*, **51**, 3223–7 (2006).
- ³⁰F. B. Zhang, Y. K. Zhou, and H. L. Li, "Nanocrystalline NiO as an Electrode Material for Electrochemical Capacitor," *Mater. Chem. Phys.*, **83**, 260–4 (2004).
- ³¹Y. Z. Zheng and M. L. Zhang, "Preparation and Electrochemical Properties of Nickel Oxide by Molten-Salt Synthesis," *Mater. Lett.*, **61**, 3967–9 (2007).
- ³²W. Xing, F. Li, Z. F. Yan, and G. Q. Lu, "Synthesis and Electrochemical Properties of Mesoporous Nickel Oxide," *J. Power Sources*, **134**, 324–30 (2004).
- ³³Y. Z. Zheng, H. Y. Ding, and M. L. Zhang, "Preparation and Electrochemical Properties of Nickel Oxide as a Supercapacitor Electrode Material," *Mater. Res. Bull.*, **44**, 403–7 (2009).
- ³⁴W. B. Ni, D. C. Wang, Z. Z. Zhao, Z. J. Huang, and J. W. Zhao, "A Novel Synthesis of Mesoporous Nickel Oxide with Excellent Cycling Stability Used in Supercapacitors," *Chem. Lett.*, **39**, 98–9 (2010). □